Quantification of the Extent and Severity of Perfusion Defects in Canine Myocardium by PET Polar Mapping

Karl T. Sun, Marc De Groof, Jeonghee Yi, Herbert W. Hansen, Kewei Chen, Johannes Czernin, Michael E. Phelps and Heinrich R. Schelbert

Division of Nuclear Medicine, Department of Molecular and Medical Pharmacology, UCLA School of Medicine and Laboratory of Structural Biology & Molecular Medicine, University of California, Los Angeles, California*

This study validates perfusion defect extent and severity as derived by PET polar maps in vivo against measurements derived from radiolabeled microspheres. **Methods:** In seven open-chest dogs, either the left anterior descending (n = 11) or left circumflex coronary artery (n = 13) were ligated sequentially from distal to proximal. After each occlusion, gated PET images were acquired with ^{13}N-ammonia (20 mCi) while radiolabeled microspheres were administered into the left atrium. The transaxial PET images were reoriented into left ventricular short-axis cuts, including the apex, and polar maps were generated from circumferential activity profiles. PET polar maps were then compared with polar maps derived from microspheres after normal databases for ^{13}N-ammonia and for microspheres were established. Nitrogen-13 or microsphere activities of less than 1.5 s.d. below the mean were defined as hypoperfused. **Results:** The extent (percent of left ventricular mass) and mean severity of the hypoperfused myocardium in the postmortem microsphere measurements ranged from 3% to 69% and 3% to 58%, respectively. The estimated extent by summed PET and by microspheres correlated by $y = 4.95 + 0.95x$ ($r = 0.91$, s.e.e. = 0.085, $p < 0.001$) and mean severity by $y = 5.52 + 0.87x$ ($r = 0.85$, s.e.e. = 0.101, $p < 0.001$). The extent and severity were similar for summed and gated PET studies. **Conclusion:** The current study validated a polar map approach that provides accurate, quantitative assessment of the extent and severity of myocardial perfusion defects in vivo. Gating did not yield an improved correlation between PET and microsphere measurements. Thus, ungated PET images can be used to assess accurately the extent and severity of perfusion defects.

Key Words: PET; polar maps; ischemia

J Nucl Med 1994; 35:2031–2040

The extent and severity of hypoperfused myocardium have prognostic significance in patients with coronary artery disease (*1–4*). Methods for quantifying the size and severity of perfusion defects are therefore useful for risk stratification of patients. At present, SPECT with ^{201}Tl or ^{99m}Tc sestamibi is used most commonly to evaluate perfusion abnormalities of the heart. PET offers an improved image quality because of a higher spatial resolution and correction for photon attenuation. Both advantages should improve the accuracy with which regional reductions in radiotracer concentrations in the human myocardium can be quantified (*5,6*).

The two-dimensional polar map display of the three-dimensional activity distribution throughout the left ventricular myocardium has been validated for SPECT in animals and serves for semiquantitative measurements of perfusion abnormalities (*7,8*). Several laboratories have adopted the polar mapping approach for use with PET (*9–11*). However, the approach for estimating the extent and severity of perfusion defects with PET remains to be validated. Moreover, it remains uncertain whether polar maps derived from gated rather than ungated PET images provide more accurate estimates of the extent and severity of perfusion abnormalities.

Thus, the aim of this study was to validate measurements of the extent and severity of perfusion abnormalities derived from PET polar maps. This was done in acute dog experiments in which the estimates derived noninvasively with PET were compared with independent measurements by microspheres and tissue counting.

METHODS

Overall Study Design

In acute, open-chest dog experiments, either the left anterior descending (LAD) or the left circumflex (LCX) coronary artery was dissected free at various sites. After positioning the animal in the PET device, ^{13}N-ammonia was injected intravenously while radiolabeled microspheres were administered into the left atrium. Gated transaxial PET images were then acquired. After decay of ^{13}N activity, a perfusion defect was created by occluding the snare located most distally on a coronary artery, followed by a second concurrent administration of ^{13}N-ammonia and microspheres and acquisition of gated PET images. This was followed by sequential, more proximal coronary occlusions to create consecutively larger

Received Jan. 25, 1994; revision accepted June 23, 1994.

For correspondence or reprints contact: Heinrich R. Schelbert, MD, Department of Molecular and Medical Pharmacology, UCLA School of Medicine, Los Angeles, CA 90024-1735.

*Operated for the U.S. Dept. of Energy by the Univ. of California under contract no. DE-FC03-87 ER 60615.

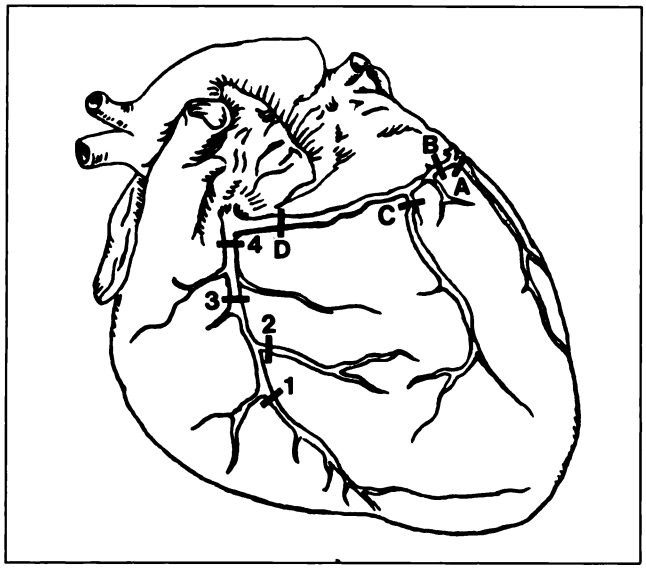

FIGURE 1. Schematic figure with sites of occlusion on the LAD artery (1–4) and LCX artery (A–D).

perfusion defects; each occlusion was followed by concurrent microsphere and ^{13}N-ammonia injections and PET imaging. The extent and severity of perfusion defects were determined postmortem by counting myocardial tissue samples for the microsphere activity concentrations and compared with the extent and severity of perfusion defects as delineated on ^{13}N-ammonia polar maps generated from reoriented short-axis cross sections of the left ventricular myocardium.

Animal Preparation

Seven mongrel dogs (14.5–33 kg, mean 22 ± 7 kg of body weight) were anesthetized with intravenous sodium thiomylal (15 mg/kg; Surital, Parke-Davis, Morris Plains, NJ). The dogs were then intubated and ventilated with a respirator. Anesthesia was maintained with a mixture of halothane (0.3%–0.4%), room air and oxygen (2 liter/min). A catheter was advanced through the femoral artery into the abdominal aorta for continuous blood pressure monitoring and for withdrawal of arterial blood. After left thoracotomy through the fifth intercostal space, the pericardium was incised widely and sutured to the chest wall, thus forming a cradle for suspending the heart. A polyvinyl catheter was inserted into the left atrium for the administration of radiolabeled microspheres.

In each dog, short, 0.5- to 1.0-cm segments of either the LAD (n = 11) or LCX (n = 13) coronary artery were dissected free at different levels of the vessel (Fig. 1). Snares were placed loosely around the dissected portions of the coronary artery. They were tightened later during the imaging protocol. The coronary artery was thus ligated sequentially from distal to proximal after each imaging procedure to create progressively larger perfusion defects for each measurement.

Experimental Protocol

The instrumented, open chest dogs were positioned in the right lateral decubitus position ("left side up") in a whole-body PET instrument (model 931/8, CTI/Siemens, Knoxville, TN), which acquires simultaneously 15 transaxial planes with an interplane spacing of 6.75 mm. The tomograph's gantry was rotated horizontally to −15° to align the tomograph's axis more closely with the long-axis of the heart and, thus, to minimize the angle of image reorientation. A 2-min rectilinear transmission scan was performed to ascertain adequate positioning of the heart within the axial field of view. Transaxial transmission images were then acquired for 20 min with a ^{68}Ga ring source for the correction of photon attenuation.

Immediately after the injection of approximately 2 × 10^6 carbonized polystyrene microspheres (diameter 15.5 ± 0.1 μ; labeled with ^{57}Co, ^{113}Sn, ^{103}Ru, ^{95}Nb and ^{46}Sc; DuPont, N. Billerica, MA), 20 mCi of ^{13}N-ammonia diluted in saline were administered as a 15-sec bolus into the left atrium. Four minutes later, gated transaxial images with eight phases per RR interval were acquired for 20 min. After completion of the baseline study, the previously placed and most distally located coronary artery snare was ligated. This was preceded by a bolus injection of lidocaine (1 mg/kg).

Fifteen minutes later, after heart rate and blood pressure had stabilized, radiolabeled microspheres were administered into the left atrium, followed immediately by a second ^{13}N-ammonia injection and gated image acquisition as described earlier. Electrocardiograms and blood pressure were monitored throughout each study using a strip chart recorder (Brush 200, Gould Inc., Cleveland, OH).

About 45 min later (after physical decay of ^{13}N activity), the next, more proximal coronary snare was tightened to create a larger perfusion defect followed 15 min later by near simultaneous administration of another set of radiolabeled microspheres and ^{13}N-ammonia and by gated PET image acquisition. As many as five consecutive imaging studies were performed in a given animal. After completion of the imaging studies, the animals were killed during deep anesthesia with concentrated KCl solution, and the hearts were excised.

Analysis of PET Data

Generation of Short-Axis Cuts of the Left Ventricular Myocardium. The image files were reconstructed on a VAX 4000 mainframe computer (Digital Equipment Corp., Maynard, MA) using a Shepp-Logan filter with a cutoff frequency of 0.25 cycles/cm, which resulted in an effective in-plane resolution of 11-mm FWHM. The summed and the gated transaxial image FWHM sets of 15 planes each were then transferred to a Macintosh II desktop computer (Apple Computer, Inc., Cupertino, CA) for further processing (*12*). The orientation of the long-axis of the left ventricle and the position of the six equidistant short-axis slices were defined by an experienced computer operator (*13*). As shown in Figure 2, spherical sampling was applied to the apical portion of the left ventricle to derive activity profiles in an orientation perpendicular to the inner border of the myocardium (*14*). The three apical cuts (slice numbers 6, 7 and 8 in Fig. 2) were sliced out around the vertex, which was positioned at one-half of the plane thickness above the most apical user-defined short-axis plane at an angle of 15°, 45° and 75° to the long-axis. Thus, the sixth, most apical "nonapical" slice was included in the first apical slice.

The reorientation and reslicing parameters that define the orientation of the short-axis images relative to the transaxial images and the interplane distance were the same for both, the summed ("ungated") and diastolic images. Ungated images were obtained by summing all eight individual frames recorded during the cardiac cycle.

Generation of Nitrogen-13-Ammonia Polar Maps. Polar maps were generated from circumferential profiles of the maximal regional myocardial activity along 60 equally spaced sectors (each six degrees). For each sector, including the three apical slices, the

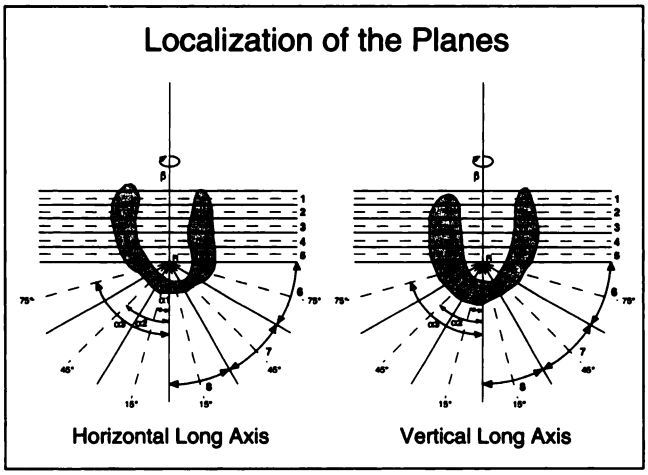

FIGURE 2. Schematic illustration of axes that were used to reslice the heart. Nonapical slices (axes 1–5) are positioned interactively, whereas apical cuts (axes 6–8) are positioned automatically by the computer program. Three apical planes are sliced out 360° (β) around a vertex (R), which is positioned at one half of the plane thickness above the most apical user-defined short-axis plane at 15° (α_1), 45° (α_2) and 75° (α_3).

myocardial wall thickness was calculated using a profile-fitting algorithm previously developed and validated in this laboratory.

This fitting algorithm, described and validated but reported in only preliminary form (*15*), uses five parameters, e.g., the internal radius of each short-axis slice, the myocardial wall thickness, the activity in the left ventricular blood pool, the myocardial activity concentration and the background activity. The algorithm yields regional recovery coefficients directly from the gated PET images, which are essential for the correction of partial-volume effects. Thus, a count activity profile corrected for partial volume can be obtained along a radial ray extending from the center of the left ventricular blood pool through the myocardial wall and background.

The polar maps were normalized subsequently by averaging the pixel values of the top 5% of the raw polar map to obtain a normalization factor that served to scale the raw polar map to a maximal value of 255, thus resulting in a "normalized polar map." This procedure diminished the influence of outliers on the normalization process.

Generation of a Normal PET Database. To define the criteria of myocardial perfusion defects, two separate databases were established for the PET polar maps generated from the summed and gated images. For the "gated" database of normals, the images of the frame with the largest diameter (diastole) of the left ventricle was chosen. Databases of normals were established from the first five dogs in the current study. Baseline polar maps of these dogs were obtained as described earlier. Average sector values (μ) and s.d. were calculated from the normalized pixel values (range 1–255) for all 480 sectors (8 planes with 60 sectors each) of the polar map. To identify hypoperfused myocardium, the adequacy of different thresholds ranging from μ − 1.0 to 2.0 s.d. at 0.25-s.d. increments was explored. The optimal threshold to define the normal limits of myocardial blood flow was found to be μ − 1.5 s.d. Values below or above the chosen value of μ − 1.5 s.d. resulted in additional perfusion defects outside the vessel of intervention or, conversely, did not identify perfusion defects that were clearly present on visual analysis. Although this threshold

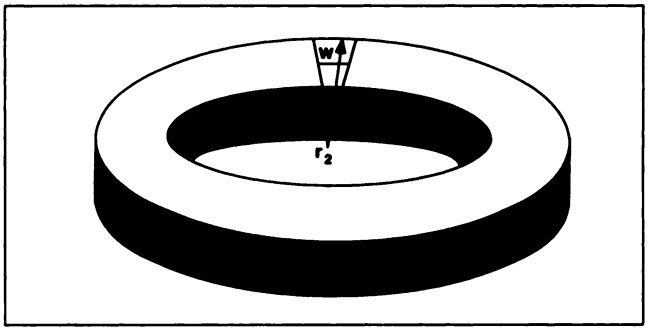

FIGURE 3. Mass of each six-degree sector was calculated by the product of wall thickness ($r_1 - r_2$) × mean width (w) × slice thickness (t) × density of myocardium.

was established largely by careful visual examination, it represented the optimal compromise between sensitivity and specificity for the detection of perfusion defects.

Determination of the Weighting Factors. To account for differences in myocardial mass between individual short-axis slices with different diameters from the base to the apex, a weighting factor was assigned to each short-axis and apical slice on the polar map. This weighting factor corrects for geometric distortions caused by the compression of the three-dimensional information into a two-dimensional format (*8,10*).

In each short-axis plane, the left ventricular myocardium was divided into 60 six-degree sectors. The area of each sector was obtained from the difference between the outer (r_1) and the inner (r_2) radii of the left ventricle (distance from the center of the left ventricular cavity to the endocardial and epicardial border of the myocardium). Divided by two, this value defines the center of the left ventricular wall. As shown in Figure 3, this point was then used to define the axial width (w) in millimeters (in the circumferential direction) of each of the six-degree sectors. The mass of each short-axis and apical slice was then estimated from the sum of the areas of all 60 sectors multiplied by the user defined slice thickness (t) and the density of the myocardium (1.05 g/cm^3), as shown in Table 1. Thus, the total mass of each slice represented the sum of all 60 sector volumes measured in absolute dimensions and corrected for density.

The relative contribution of each slice to the total left ventricular mass, as displayed on the polar map, was expressed as a fraction of 1.0 (defined as the weighting factor). A value of 1 was assigned to the short-axis cross section with the greatest mass. The weighting factor declined in proportion to the decrease in the mass of each cross section relative to the cross section with the greatest mass. The weighting factors were calculated for the summed images (Table 2) and gated images.

Calculation of Defect Extent and Severity. To calculate the extent of a perfusion defect in a specific plane, the number (n) of sectors (s) in a given plane with activity concentrations less than 1.5 s.d. below the mean multiplied by their individual masses were divided by the total number of sectors per plane (N), i.e., 60, where each sector was multiplied again by its corresponding mass (m_i).

$$\% \text{ defect/plane} = \frac{n(s \cdot m_i)}{N(s \cdot m_i)}. \qquad \text{Eq. 1}$$

To calculate the extent of a perfusion defect as a fraction of the entire left ventricular myocardium (LV), the number (n) of sectors

TABLE 1
Volumes of Each Short-Axis Slice as Estimated by PET and the True Mass Obtained from the Tissue Samples of the Five Dogs in the Normal Database

Plane	1	2	3	4	5	Mean	s.d.
1	7.5	14.7	19.4	12.5	12.9	13.4	4.3
2	8.1	14.9	22.6	13.5	14.8	14.8	5.2
3	8.9	15.5	25.3	14.3	14.6	15.7	6.0
4	8.8	14.9	21.3	14.2	14.8	14.8	4.4
5	7.8	12.8	18.2	13.8	13.9	13.3	3.7
6	12.4	12.0	12.0	16.7	16.3	13.9	2.4
7	7.4	6.7	5.8	10.2	10.2	8.1	2.0
8	2.5	1.8	2.0	4.1	3.9	2.9	1.1
Total volume (cm^3)	63.4	93.4	126.6	99.3	101.4	96.8	22.6
Estimated mass (g)	66.6	98.1	132.9	104.3	106.5	101.7	23.7
True mass (g)	70.6	78	125.4	112.8	117.8	100.9	24.8

(s) with activity concentrations less than 1.5 s.d. below the mean of normal were multiplied by the weighting factors of that plane (W) and then divided by the sum of all sectors (N) multiplied by their corresponding weighting factor (f_i):

$$\% \text{ defect/LV} = \frac{\sum n(s \cdot W)}{\sum N(s \cdot f_i)}. \quad \text{Eq. 2}$$

The average reduction of blood flow ("mean severity") in the hypoperfused mass within the entire left ventricle was calculated by:

$$\text{Mean severity} = \sum \left(1 - \frac{\text{value}_{\text{hypoperfused}}}{\text{threshold value}}\right) / n_{\text{hypoperfused}}. \quad \text{Eq. 3}$$

The $\text{value}_{\text{hypoperfused}}$ refers to the sector value of a hypoperfused sector (i.e., sector with a count value below the threshold value). The threshold value was calculated from the mean of all sector values of the entire heart minus 1.5 s.d., as described earlier, i.e., sectors with values above this threshold value are considered to be normally perfused, whereas sectors with values below this threshold are hypoperfused. The term $n_{\text{hypoperfused}}$ refers to the total number of hypoperfused sectors.

To investigate whether the use of individual weighting factors determined for each study or each dog would improve the estimates obtained by an average weighting factor, the following approach was used: (1) weighting factors were calculated for each image set; (2) average weighting factors were derived from all image sets obtained in an individual dog (i.e., the weighting factors derived from the two to five studies in a given dog were averaged for each plane and applied to all studies obtained in the same animal; and (3) a set of mean weighting factors was derived from the baseline studies in all five dogs.

Analysis of Microsphere Data

Generation of Normal Database. Corresponding to the reslicing procedure of the transaxial PET images, which results in five user-defined nonapical short-axis slices and the apex, the excised hearts were sliced into the same number of short-axis cross sections of equal thickness. After the slices were photographed, the right ventricular free wall, the nonmuscular structures of the mitral valve (i.e., leaflets, chordae and valvular ring) and epicardial fat were carefully removed. Each slice was then weighed and cut into 0.4- to 1.0-g transmural sections. The most apical, cone-shaped slice was also cut in a radial fashion into transmural sections. The localization of each section of tissue within a slice was drawn on the photograph. Each tissue sector was then well-counted for its microsphere activity concentration (*16*).

According to the localization and the contribution of each tissue sample to the total weight of the corresponding slice, each piece of tissue was assigned a certain position and proportionate number of sectors in a polar map of the microsphere activity distributions (Fig. 4). A normalization was then performed analogous to the ^{13}N-ammonia polar map procedure, thus resulting in a normalized microsphere polar maps. The average sector values (μ) and s.d. were calculated for each sector of the entire polar map. They were derived from baseline studies in each of the five dogs together with data from an additional three open chest dogs used for a different study protocol and were assembled into a normal database. A

TABLE 2
Weighting Factors as Assessed by the Profile-Fitting Algorithm for All Five Dogs of the Normal Database

Plane	1	2	3	4	5	Mean
1	0.61	0.95	0.77	0.75	0.79	0.85
2	0.66	0.97	0.89	0.81	0.91	0.94
3	0.72	1.00	1.00	0.86	0.90	**1.00**
4	0.72	0.96	0.84	0.85	0.91	0.94
5	0.63	0.83	0.72	0.83	0.85	0.85
6	1.00	0.78	0.47	1.00	1.00	0.88
7	0.60	0.44	0.23	0.61	0.63	0.51
8	0.20	0.12	0.80	0.24	0.24	0.18

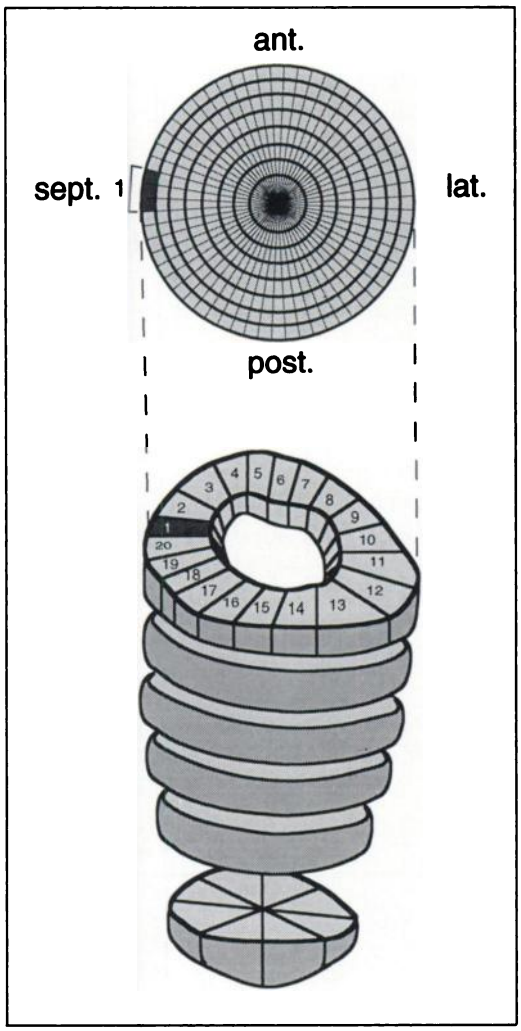

FIGURE 4. Illustration of method used to generate a normal database for the microsphere data. Each piece of tissue was assigned a certain position and number of sectors in the polar map according to the localization and the weight contribution to the whole slice.

sector value within 1.5 s.d. of the mean was considered to be normal.

Analysis of the Intervention Studies. Polar maps were generated and normalized for each intervention study in the same manner as described earlier. Tissue samples with pixel values below μ − 1.5 s.d. were then determined, and the percentage of hypoperfused myocardium was calculated by dividing the weight of hypoperfused tissue by the total mass of the left ventricle (Eq. 1 and 2). The mean severity of the hypoperfused mass was calculated by Equation 3, as described earlier. Figure 5 depicts polar maps in one dog at baseline and after four consecutive occlusions of the LCX coronary artery after a pixel-by-pixel comparison between normalized polar maps and the database of normals.

Statistical Analysis

Weighted least-squares regression analysis was used to compare the extent and severity of hypoperfused myocardium as determined by microspheres to those derived from the PET polar maps. Analysis of variance was used to determine statistical significant differences between groups of data. Differences in slope and intercept of the regression lines were assessed by the F test

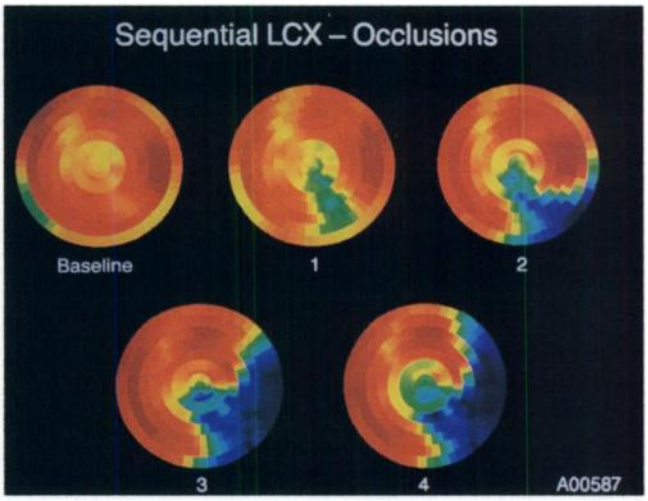

FIGURE 5. Normalized ^{13}N-ammonia polar maps of same dog at baseline and after each sequential occlusion of the LCX artery (corresponding studies 27–31 in Table 2).

(*17*). A probability value of less than 0.05 was considered statistically significant.

RESULTS

Total counts of 60 to 80 million per study or 7.5 to 10 million per gated image frame were routinely achieved for the 20 min of image acquisition. These count rates are about 100% higher than achieved for the last frame (15 min) in human studies for a ^{13}N-ammonia dose of 20 mCi (*18*).

Estimates of the left ventricular mass by PET correlated with the postmortem measurements of the left ventricular mass for the five dogs that were included in the database. The true left ventricular mass in the five dogs averaged 100.9 ± 24.8 g compared with 101.7 ± 23.7 g, as determined by PET. Although the correlation between estimated and true mass did not achieve statistical significance ($p = 0.06$), probably because of the small sample size, the close agreement between measured and PET estimated left ventricular masses confirms the accuracy of the profile fitting algorithm (Fig. 6). Despite the nearly identical mean values, however, Figure 6 indicates disparities between measurements by the two approaches in individual dogs.

Tables 3 and 4 list the extent and mean severity of perfusion defects for all studies. The small defects observed in the baseline studies in the territories of the coronary artery that was subsequently occluded most likely resulted from alterations caused by dissection and manipulation of that coronary artery prior to the PET imaging. Similar defects were noted on the microsphere data. Other possible explanations, although less likely, include the known heterogeneity of regional myocardial blood flow (*19,20*).

The extent of perfusion defects by microspheres ranged from 3% to 69%, and the mean severity ranged from 3% to 58%. The defect extent averaged 36.7% ± 24.3% in dogs with defects in the territory of the LAD and 24.6% ± 9.9% in dogs with defects in the LCX territory. The average size

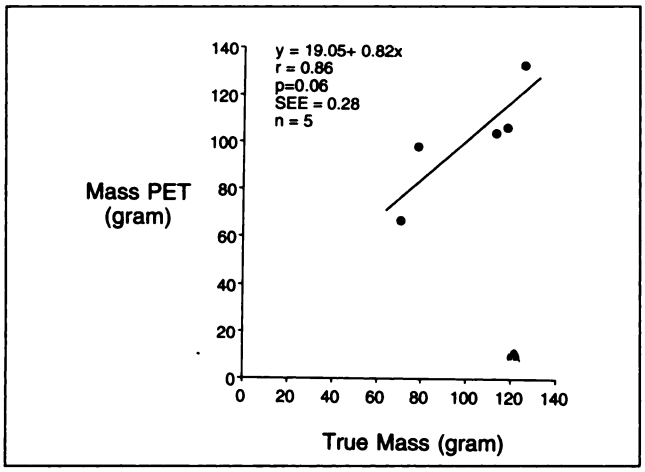

FIGURE 6. Correlation between estimated left ventricular mass by PET and directly measured values.

did not differ significantly between the two vascular territories. In one animal, defects were created in both the LAD and LCX territory with a total defect extent of 54%. Defects determined by ^{13}N-ammonia from ungated images and using mean weighting factors ranged in extent from 3% to 63% and in mean severity from 1% to 64%, respectively. The extent of defects in the LAD territory averaged 33.9% ± 25% and in the LCX coronary artery territory 26.8% ± 13.7% (p = not significant vs. microspheres). There was no significant difference in the goodness of estimation between LAD and LCX territory by PET (F ratio = 0.58, p = not significant). Moreover, the correlation between the noninvasively and invasively determined extent and severity of perfusion defects did not differ significantly between individual dogs.

Figure 7A depicts the correlation between extent of defects determined from ungated PET images and from the microsphere data, using a mean weighting factor for each of the slices. The defect extent, as derived by

TABLE 3
Extent of Perfusion Defects as Assessed by Microspheres and by PET for All Studies by Using Individual (for Each Study or Each Dog) and Mean Weighting Factors

Study	Vessel	Extent MS	Gated WF (Each study)	Gated WF (Each dog)	Gated mean WF	Summed WF (Each study)	Summed WF (Each dog)	Summed mean WF
1	Baseline	4	10	9	10	8	6	5
2	LAD	6	13	14	10	11	14	14
3	LAD	30	39	49	37	39	48	34
4	LAD	35	43	56	45	42	56	43
5	LAD	63	72	79	72	60	71	60
6	Baseline	3	5	5	5	4	5	3
7	LCX	17	33	35	31	32	34	28
8	Baseline	13	4	4	2	9	18	16
9	LCX	22	25	25	21	18	18	17
10	LCX	11	18	30	21	10	18	18
11	LCX	24	34	45	34	34	41	35
12	Baseline	15	6	6	7	4	6	14
13	LAD	32	30	33	27	28	36	29
14	LAD	60	46	51	68	44	54	64
15	LAD	69	58	68	64	60	71	64
16	LAD	67	*	*	*	55	66	63
17	Baseline	4	0	1	0	1	0	1
18	LAD	8	7	9	6	7	10	8
19	LAD	10	10	11	11	12	13	13
20	LAD	24	39	41	36	38	41	36
21	LAD + LCX	54	55	63	57	58	66	63
22	Baseline	14	29	29	24	23	23	22
23	LCX	12	26	25	20	22	21	19
24	LCX	18	27	26	21	22	22	19
25	LCX	34	36	38	27	29	31	25
26	LCX	40	52	54	50	59	58	49
27	Baseline	15	21	21	8	19	19	9
28	LCX	17	30	30	26	31	31	27
29	LCX	32	35	35	37	39	38	42
30	LCX	31	43	43	38	47	47	40
31	LCX	37	50	52	46	53	55	52

*Study not analyzed because of low counts.
MS = microspheres; WF = weighting factor.

TABLE 4
Mean Severities as Assessed by Microspheres and by PET for All Studies by Using Individual (for Each Study or Each Dog) and Mean Weighting Factors

Study	Vessel	Severity MS	Gated WF (Each study)	Gated WF (Each dog)	Gated mean WF	Summed WF (Each study)	Summed WF (Each dog)	Summed mean WF
1	Baseline	3	2	3	2	2	1	1
2	LAD	16	23	26	26	28	28	26
3	LAD	40	42	47	41	47	51	50
4	LAD	56	51	56	47	54	57	53
5	LAD	58	57	58	42	63	67	54
6	Baseline	3	6	7	3	6	5	3
7	LCX	50	39	36	45	40	38	47
8	Baseline	10	2	4	1	4	5	3
9	LCX	14	14	12	15	8	10	9
10	LCX	15	11	13	9	8	6	8
11	LCX	41	41	35	39	43	36	39
12	Baseline	8	2	2	2	2	2	2
13	LAD	14	13	14	12	8	9	10
14	LAD	25	27	29	27	26	27	28
15	LAD	44	50	56	57	46	53	56
16	LAD	52	*	*	*	64	66	63
17	Baseline	9	0	1	0	1	0	0
18	LAD	12	4	5	8	5	5	6
19	LAD	23	17	16	15	16	17	14
20	LAD	20	20	20	21	23	23	23
21	LAD + LCX	44	50	52	48	53	54	50
22	Baseline	16	21	21	25	23	23	27
23	LCX	20	21	20	24	21	20	27
24	LCX	21	25	24	24	25	24	28
25	LCX	22	22	23	28	24	26	30
26	LCX	45	41	42	42	43	43	45
27	Baseline	16	8	8	3	7	7	4
28	LCX	24	18	18	11	16	16	11
29	LCX	43	29	27	26	29	28	25
30	LCX	56	46	43	45	45	44	45
31	LCX	54	49	46	47	48	47	47

*Study not analyzed because of low counts.
MS = microspheres; WF = weighting factor.

PET, was closely correlated with the extent measured with radiolabeled microspheres ($y = 4.95 + 0.95x$, $r = 0.91$. $p < 0.0001$, s.e.e. = 0.085). Figure 8A depicts the relationship between measured and estimated mean severities.

Figures 7B and 8B show the defect extent and severity using gated PET images for the same weighting factors. Figures 7C and 8C compare the extent and severity of defects obtained from gated images using individual weighting factors for each study. One gated intervention could not be analyzed because of poor image quality as a result of low counts after the administration of a lower tracer dose.

As depicted in Figures 7 and 8, different weighting factors did not affect the relationship between PET and microsphere measurements. Similarly, ungated and gated PET studies yielded comparable correlations with microspheres. There were no significant differences for the determination of defect extent in terms of slopes and intercepts between gated and ungated (F ratio = 0.087, p = not significant) or between mean weighting and individual weighting factors.

DISCUSSION

Although the polar map approach has already been used for investigational or clinical purposes, this study validates for the first time its use for PET measurements of the extent and severity of perfusion defects. The use of appropriate weighting factors that correct for differences in the slice sizes and the inclusion of the left ventricular apex account for the accuracy of such measurements, as confirmed by independent measurements with microspheres and postmortem tissue determinations of the regional activity concentrations.

Study Limitations

There are several limitations to this study. The current approach was tested only for the territories of the LAD and the LCX coronary arteries. It is important to note that there were no significant territory-specific differences in

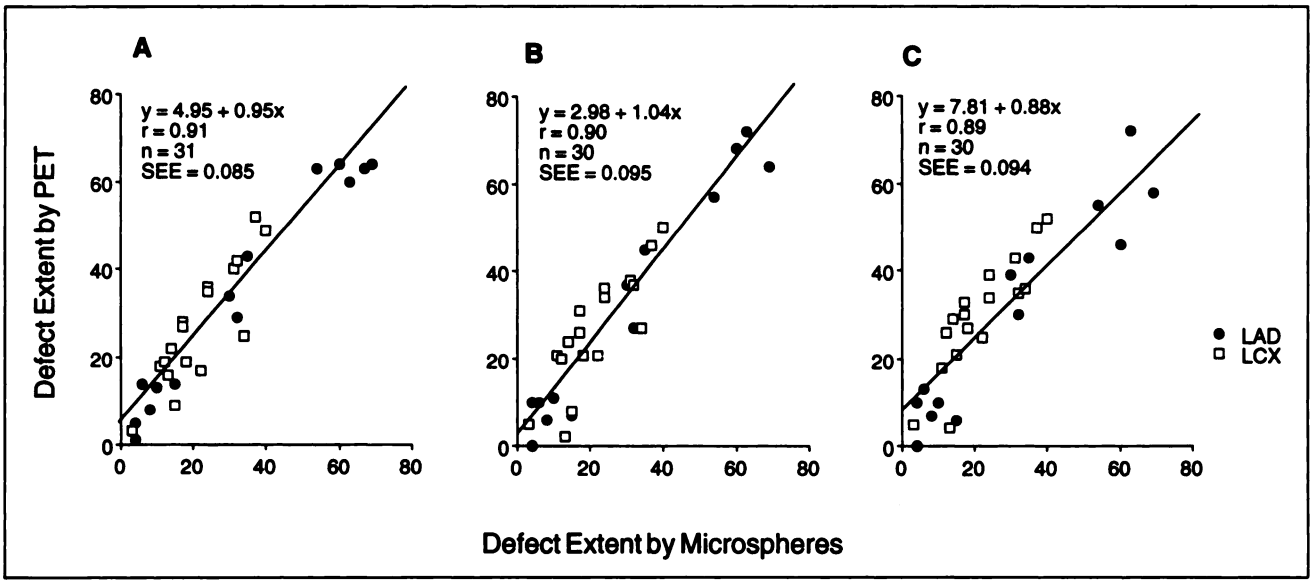

FIGURE 7. Correlation between perfusion defect extent obtained by microspheres and summed PET images using a set of average weighting factors derived from all five dogs in the normal database (A), using gated studies and mean weighting factors for each dog (B) and using gated studies with individual weighting factors for each study, i.e., calculated individually for each image set (C). Correlations between measured and PET estimated extents are not significantly different from each other.

the correlation between microsphere-measured and PET-derived measurements of perfusion defect extent and severity. Although no studies were performed for the territory of the right coronary artery because of its small size and the related difficulties in surgical preparation (*21*), the absence of systematic differences between the LCX and the LAD coronary artery territories makes it unlikely that the application of the polar map approach to the right coronary artery territory would have yielded different results.

Weighting factors derived from the calculation of the myocardial volume of the short-axis and apical slices were obtained through a profile-fitting algorithm, which depends on the detection of the highest activity within a given myocardial region. In larger defects, when there is little or no tracer activity in the abnormal area, the current approach might lead to a fitting error. This could result in an under- or overestimation of the true myocardial mass or the defect size. However, this limitation plays a role only when individual weighting factors are used for each study because the mean weighting factors are derived from baseline studies without perfusion defects. Such baseline studies, however, are not available in patients. This necessitates the use of weighting factors from a normal database

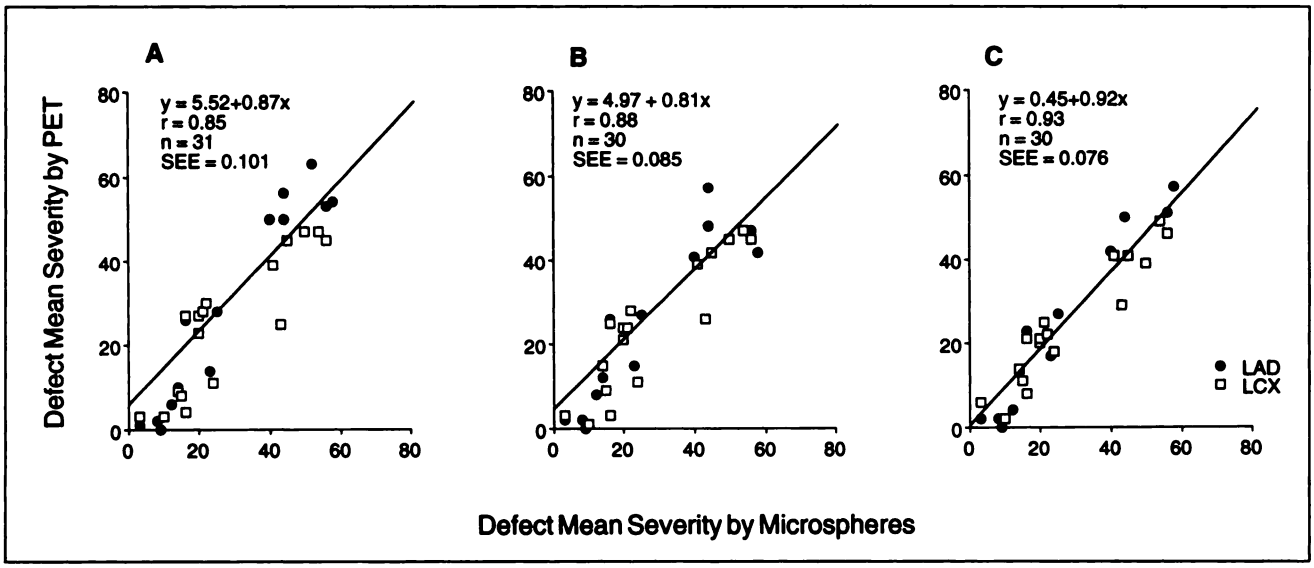

FIGURE 8. Correlation between mean severity obtained by PET images and microsphere data using same sets of weighting factors as for the calculation of extents (Fig. 7A–C). There are no significant differences between these correlations.

derived from a group of normal volunteers. However, the close agreement between microsphere and PET measurements based on average weighting factors suggests that valid estimates of perfusion defect can be obtained in such patients.

Like most other studies that attempted to quantify the extent and severity of perfusion abnormalities, the present study was performed in an animal model of acutely infarcted myocardium (*22,23*). In this model, the thickness of the myocardium is preserved, and adjacent myocardium is normal. In the clinical setting, however, hypoperfused (infarcted or ischemic) myocardium frequently can be distinguished with less certainty from normal myocardium. Also, the wall thickness in infarcted areas with extensive scar formation may be reduced (*24*). Estimation of myocardial activity concentrations in such regions may then be limited or even impossible because of the partial-volume effect, which leads to an underestimation of the observed myocardial activity (*25*). No appropriate fitting algorithms are currently available for PET or SPECT that would correct appropriately for such potential errors in severely hypoperfused myocardium. However, this problem can be solved by direct measurements of wall thickness with MRI or echocardiography.

Technical Considerations

To account for differences in myocardial mass for each short-axis cut from base to apex, average and individual (for each dog and for each study) weighting factors were used. The results indicate that average weighting factors yielded estimates that did not differ significantly from those obtained by individual weighting factors. The most likely explanations for these observations are the relatively well-preserved geometric shape of the hearts and the normal wall thickness in these acute studies.

Ungated images, as used most frequently in the clinical setting, contain the blurring effect of cardiac motion; this might cause errors in estimating the extent and severity of perfusion defects. Gating, therefore, offers a theoretical advantage of more accurate measurements of perfusion abnormalities. One of the goals of this study was therefore to explore this theoretical advantage by comparing estimates obtained from gated and from summed (nongated) images.

The results demonstrate no clear advantage of gated image acquisition. This may be a result of the particular approach used to calculate myocardial mass by PET. The profile-fitting algorithm currently used in the authors' computer program is based on the detection of regions with the highest tracer activity. Thus, profiles from regions with extremely low activities cannot be obtained. In these cases, the wall thickness is estimated by extrapolation of adjacent regions with higher activities and, thus, higher perfusion. Furthermore, the defect extent derived from the PET images is expressed as a percentage of the total left ventricular mass. Thus, the same blurring effect on ungated images applies to normal and to hypoperfused myocardium equally. This most likely offsets the advantage of gating because the ratio between the mass of hypoperfused to the total mass of the myocardium remains constant.

In addition, the theoretical advantage of gated image acquisition for measurements of defect sizes would be less in humans for two reasons. One is the lower heart rate compared with heart rates of 145 ± 20 beats/min in the current acute dog experiments. A second and even more important reason is the lower count density of gated images in humans. For example, in the current study, 20 mCi of ^{13}N-ammonia was given in 22 ± 7-kg dogs. A similar dose would be administered in humans of weights three or four times as large so that considerably lower count rates would be acquired. Therefore, the resulting image noise would offset any advantage by gating.

In comparison to previously published validation studies for SPECT polar maps (*7,8*), a slightly better correlation was found between the estimated and measured perfusion defect extent. This difference is most likely due to the aforementioned absence of a satisfactory method for photon attenuation correction in SPECT and of the better spatial resolution of PET and is consistent with previously published data (*5,6*).

CONCLUSION

The quantitation of perfusion defect plays an important role in the clinical setting because it helps to assess the effect of medical treatment, angioplasty and surgical revascularization.

The current study validated a new polar map approach that provides accurate, quantitative assessment of the extent and severity of myocardial perfusion defects in vivo. Furthermore, gating did not yield an improved correlation between PET and microsphere measurements. Thus, ungated PET images can be used to accurately assess the extent and severity of perfusion defects in humans, which should be useful in the clinical management of patients with acute or chronic coronary artery disease.

ACKNOWLEDGMENTS

The authors thank Ron Sumida, Larry Pang, Francine Aguilar, Der-Jenn Liu, Marc Hulgan, Gloria Stocks and Judy Edwards for their excellent technical assistance; the staff of the Medical Cyclotron at UCLA for providing the isotopes; Dr. James Sayre, Arion Chatziioannou, Carl Selin and Tony Ricci for assistance with data analysis; Diane Martin and Wendy Wilson for preparation of the illustrations; and Eileen Rosenfeld and Judy Amos for secretarial assistance.

This work was supported in part by the Director of the Office of Energy Research, Office of Health and Environmental Research (Washington, DC), by research grants 29845 and 33177, National Institutes of Health (Bethesda, MD) and by an Investigative Group Award by the Greater Los Angeles Affiliate of the American Heart Association (Los Angeles, CA). Presented in part at the 42nd Annual Scientific Session of the American College of Cardiology (Anaheim, CA) in 1993 and at the 40th Annual Meeting of the Society of Nuclear Medicine (Toronto, Canada) in 1993.

Karl T. Sun is the recipient of a stipend from the Swiss National Science Foundation.

REFERENCES

1. Sobel BE, Bresnahan GF, Shell WE, Yoder RD. Estimation of infarct size in man and its relation to prognosis. *Circulation* 1972;46:640–648.
2. Alonso DR, Scheidt S, Post M, Killip T. Pathophysiology of cardiogenic shock. Quantification of myocardial necrosis, clinical, pathological and electrocardiographic correlations. *Circulation* 1973;48:588–596.
3. Ladenheim M, Pollock V, Rozanski A, et al. Extent and severity of myocardial hypoperfusion as predictors of prognosis in patients with suspected coronary artery disease. *J Am Coll Cardiol* 1986;7:464–471.
4. Yoshida K, Gould K. Quantitative relation of myocardial infarct size and myocardial viability by positron emission tomography to left ventricular ejection fraction and 3-year mortality with and without revascularization. *J Am Coll Cardiol* 1993;22:984–997.
5. Go R, Marwick T, MacIntyre W, et al. A prospective comparison of rubidium-82 PET and thallium-201 SPECT myocardial perfusion imaging utilizing a single dipyridamole stress in the diagnosis of coronary artery disease. *J Nucl Med* 1990;31:1899–1905.
6. Stewart R, Kalus M, Molina E, et al. Rubidium-82 PET versus thallium-201 SPECT for the diagnosis of regional coronary artery disease. *Circulation* 1989;80:II-209.
7. Caldwell J, Williams D, Harp G. Quantitation of size of relative myocardial perfusion defect by single photon emission computed tomography. *Circulation* 1984;70:1048–1056.
8. Prigent F, Maddahi J, Garcia EV, et al. Comparative methods for quantifying infarct size by thallium-201 SPECT. *J Nucl Med* 1987;28:325–333.
9. Hicks K, Ganti G, Mullani N, Gould KL. Automated quantitation of three-dimensional cardiac positron emission tomography for routine clinical use. *J Nucl Med* 1989;30:1787–1797.
10. Porenta G, Kuhle W, Czernin J, et al. Semiquantitative assessment of myocardial viability and perfusion utilizing polar map displays of cardiac PET images. *J Nucl Med* 1992;33:1623–1631.
11. Laubenbacher C, Rothley J, Sitomer J, et al. An automated analysis program for the evaluation of cardiac PET studies: initial results in the detection and localization of coronary artery disease using nitrogen-13-ammonia. *J Nucl Med* 1993;34:968–978.
12. Ratib O, Huang H, Schelbert H. A software for quantitative analysis of cardiac images on a Macintosh computer. *J Am Coll Cardiol* 1990;15:269A.
13. Porenta G, Kuhle W, Czernin J, et al. Interactive user-friendly image analysis of cardiac PET images on a low cost desktop computer. In: Murray A, ed. *Proceedings computers in cardiology*. Los Alamitos, CA: IEEE Computer Society Press; 245–248.
14. De Groof M, Khanna S, Maddahi J, et al. Development of an objective computerized quantitative method to improve assessment of myocardial N-13 ammonia stress perfusion imaging in PET. *J Nucl Med* 1992;33:1009.
15. Porenta G, Kuhle W, Sinha S, et al. Gated PET FDG imaging permits parameter estimation of cardiac geometry: validation using gated MR imaging and echocardiography. *J Nucl Med* 1991;32:927.
16. Heymann MA, Payne BD, Hoffman JIE, Rudolph AM. Blood flow measurements with radionuclide-labeled particles. *Prog Cardiovasc Dis* 1977; 20:55–79.
17. Snedecor G, Cochran W. *Statistical methods*, 7th edition. Ames, Iowa: The Iowa State University Press; 1982:385–388.
18. Chan S, Brunken R, Phelps M, Schelbert H. Use of the metabolic tracer carbon-11-acetate for evaluation of regional myocardial perfusion. *J Nucl Med* 1991;32:665–672.
19. King RB, Bassingthwaighte JB. Temporal fluctuations in regional myocardial flows. *Pfluger Arch* 1989;413:336–342.
20. Flynn AE, Coggins DL, Austin RE, et al. Nonuniform blood flow in the canine left ventricle. *J Surg Res* 1989;49:379–384.
21. Scheel KW, Ingram LA. Relationship between coronary collateral growth in the dog and ischemic bed size. *Basic Res Cardiol* 1981;76:305–312.
22. Keyes JW, Brady TJ, Leonard PF. Calculation of viable and infarcted myocardial mass from thallium-201 tomograms. *J Nucl Med* 1981;22:339–343.
23. Narahara KA, Thompson CT, Maublant JC, Brizendine M, Mena I. Thallium-201 single-photon emission tomography estimates of left ventricular mass in patients with and without ischemic heart disease. *Am Heart J* 1987;114:84–90.
24. Perrone-Filardi P, Bacharach SL, Dilsizian V, et al. Regional left ventricular wall thickening. Relation to regional uptake of 18 fluorodeoxyglucose and ^{201}Tl in patients with chronic coronary artery disease and left ventricular dysfunction. *Circulation* 1992;86:1125–1137.
25. Parodi P, Schelbert HR, Schwaiger M, et al. Cardiac emission computed tomography: underestimation of regional tracer concentrations due to wall motion abnormalities. *J Comput Assist Tomogr* 1984;8:1083–1092.